JOURNAL OF COMPUTATIONAL PHYSICS 121, 79–93 (1995)

Genuinely Multidimensional Upwinding for the 2D Shallow Water Equations*

P. GARCIA-NAVARRO,† M. E. HUBBARD, AND A. PRIESTLEY

Department of Mathematics, P.O. Box 220, University of Reading, Whiteknights, Reading, United Kingdom

Received May 3, 1994; revised February 21, 1995

A multidimensional upwinding technique is applied to the simulation of 2D shallow water flows. It is adapted from fluctuation splitting methods recently proposed for the solution of the Euler system of equations on unstructured triangular grids. The basis of the numerical method is stated and the particular adaptation to the shallow water system is described. Numerical results of interest to hydraulic engineers are presented. Despite the complexities, advantages related to the use of a discretisation based on triangles would seem to make the schemes competitive with those currently in use.

1. INTRODUCTION

In reading the literature of recent years on the latest advances in numerical methods for hyperbolic conservation laws, one might gain the impression that many more people worked on problems involving the Euler equations than on problems concerning the shallow water equations. In practice, though, this is not the situation, with many more engineers, physicists and mathematicians being involved in solving problems of the latter kind on a day to day basis.

Classical methods and central difference schemes still dominate the commercial software products for this market, with Preissmann's, Abbott's (see [4], for example), and McCormack's [7] schemes the most commonly used. These schemes are well known to require special treatment in many situations so that the calculations may proceed.

Some years after their adoption for solving problems in gas dynamics, upwind and TVD (total variation diminishing) numerical schemes have been successfully used for the solution of the shallow water equations, with similar advantages [8]. Their use is nevertheless only gradually gaining acceptance in this sector.

Recently, in the context of gas dynamics, doubt has been expressed as to whether the essentially 1D TVD schemes are the most suitable choice for multidimensional calculations, and the search has been initiated for genuinely multi-dimensional approaches. Most of these are based on piecewise constant representations of the solution on triangular grids with a 1D upwinding of the Riemann problem for each edge of the triangle. However, it has been claimed that such an approach is weak when the solution is not constant along a triangle edge, since it may misinterpret features which are not aligned with grid interfaces.

In a different philosophy, instead of concentrating on finite volumes and the changes of the variables across the cell sides, Deconinck *et al.* [5] consider solutions on triangular grids in which the unknowns are associated with the vertices and updates to these nodal values are through the advection of linear wave solutions. This avoids the problems of taking the normal to the cell interfaces as a privileged direction.

Reference [5] is concerned with gas dynamics applications. In this paper we consider the use of this technique for 2D shallow water flows and the question of whether they may be of practical use. In the next sections, the basis of the numerical method is stated and the adaptation to the shallow water system is described. The numerical treatment of the boundaries as well as the inclusion of source terms in the governing equations are also discussed. Finally, some numerical results are presented. Although this work is at an early stage, our results indicate that the advantages may outweigh the disadvantages and that these schemes may have a future for hydraulic engineering applications.

2. BASIC TECHNIQUE

2.1. *Scalar Case*

For the numerical solution of the 2D linear scalar equation

$$\frac{\partial w}{\partial t} + \mathbf{a} \cdot \nabla w = 0, \quad \mathbf{a} = (a_x, a_y), \tag{2.1}$$

with constant $\mathbf{a}$, we assume the given physical domain to be discretised by triangular cells and a set of initial values w_i stored at the nodes of the mesh. For each cell T, of area S_T, a cell fluctuation is defined as

* The first author was funded by the EC Program of Human Capital and Mobility, the second by DRA Farnborough, and the third by the U.K. S.E.R.C.

† On leave from the University of Zaragoza.

0021-9991/95 $12.00

$$\Phi_T = \int_T \frac{\partial w}{\partial t} dS \tag{2.2}$$

and a cell residual R_T as

$$R_T = -\frac{1}{S_T}\Phi_T = \frac{1}{S_T}\int_T \mathbf{a}\cdot\nabla w dS = -\frac{1}{S_T}\oint w\mathbf{a}\cdot\mathbf{n} dC, \tag{2.3}$$

where C represents the cell boundary and $\mathbf{n}$ is the inward unit normal to the cell boundary. The cell fluctuation or cell residual contains information on the state of the cell to be transmitted to w over a time step, so that the changes made to the values of the w_i's at the nodes of triangle T will be proportional to Φ_T or R_T. The distribution of the information to the nodes should, if possible, be done in a way which ensures conservation [15].

From the properties of the normals in the cell and the additional assumption that the solution varies linearly within each element, it is possible to identify a discrete approximation of ∇w, where $\mathbf{n}_i$ is the normal to the edge opposite node i,

$$\nabla w_T = \frac{1}{2S_T}\sum_{i=1}^{3} w_i \mathbf{n}_i \tag{2.4}$$

such that

$$R_T = \mathbf{a}\cdot\nabla w_T, \tag{2.5}$$

or

$$\Phi_T = -\sum_{i=1}^{3} w_i k_i \tag{2.6}$$

with the introduction of the quantities

$$k_i = \tfrac{1}{2}\mathbf{a}\cdot\mathbf{n}_i \tag{2.7}$$

which contain information about the direction of advection relative to the cell. They can be used to decide whether flow enters or leaves the triangle through a particular edge and, in that sense, are a useful tool for the upwind properties of the technique.

Residuals and fluctuations are cell-based quantities which are going to be used for the updating of the nodal values. For this purpose we introduce distribution coefficients, D_T^i, defining the weightings of the residual to the nodes in a cell. For conservation and consistency they must satisfy

$$\sum_{i=1}^{3} D_T^i = 1$$

in every cell; see [5], for example. Then, a first-order explicit time-stepping procedure at the nodes can be defined as

$$w_i^{n+1} = w_i^n - \frac{\Delta t}{S_i}\left[\sum_{T_i} S_T D_T^i R_T^n\right], \tag{2.8}$$

where the sum is over all the cells meeting at node i, and where $S_i = \frac{1}{3}\sum_{T_i} S_T$. In order to focus on the individual cell treatment, the advection scheme can be expressed, on each triangle, as

$$S_1 w_1^{n+1} = S_1 w_1^n - \Delta t S_T D_T^1 R_T^n$$
$$S_2 w_2^{n+1} = S_2 w_2^n - \Delta t S_T D_T^2 R_T^n$$
$$S_3 w_3^{n+1} = S_3 w_3^n - \Delta t S_T D_T^3 R_T^n,$$

where only the influence from the individual triangle has been included.

There exist many criteria for the design of advection schemes, depending on the choice of the distribution coefficients. Two properties are of interest, positivity and linearity preservation of the scheme. The former is related to the 1D property of monotonicity whilst the second has to do with the accuracy of the method. Unfortunately, their simultaneous requirement is incompatible with the linearity of a scheme. This leads to the generation of non-linear advection schemes, even for linear equations. These schemes are based on the construction of advection speed vectors $\mathbf{a}_m$ in the direction of the local gradient, defined as

$$\mathbf{a}_m = a_m \mathbf{m}$$

with

$$\mathbf{m} = \frac{\nabla w}{|\nabla w|}, \quad a_m = \mathbf{a}\cdot\mathbf{m}.$$

This makes the coefficients k_i of (2.7) dependent on the solution, enabling the simultaneous satisfaction of the two desired properties. Note that the use of the frontal speed $\mathbf{a}_m$ does not alter the cell residual, since

$$\mathbf{a}\cdot\nabla w = \mathbf{a}_m\cdot\nabla w.$$

If the equation to be solved is non-linear, a suitable linearization must be performed before the techniques described for the linear equation are applied.
Given the non-linear equation

$$\frac{\partial w}{\partial t} + \nabla\cdot\mathbf{F}(w) = 0, \quad \mathbf{F} = (F, G),$$

where

$$\mathbf{a} = (F_w, G_w),$$

the fluctuation is defined as

$$\Phi_T = -\int_T \nabla \cdot \mathbf{F} dS.$$

An averaged advection speed which satisfies discrete conservation can now be found by assuming linear variation of w over the cell and therefore constant gradient ∇w. In that case

$$\int_T \nabla \cdot \mathbf{F} dS = \int_T (F_x + G_y) dS = \int_T (F_w w_x + G_w w_y) dS$$
$$= w_x \int_T F_w dS + w_y \int_T G_w dS = (\bar{a}_x w_x + \bar{a}_y w_y) S_T$$

where

$$\bar{a}_x = \frac{1}{S_T}\int_T F_w dS, \quad \bar{a}_y = \frac{1}{S_T}\int_T G_w dS,$$

and

$$\Phi_T = -S_T \bar{\mathbf{a}} \cdot \nabla w, \quad k_i = \tfrac{1}{2}\bar{\mathbf{a}} \cdot \bar{\mathbf{n}}_i,$$

with

$$\bar{\mathbf{a}} = (\bar{a}_x, \bar{a}_y).$$

Since the advection schemes used for the shallow water equations are no different from those used for the Euler equations we will not go into further detail about their particular construction and description. We refer the reader to the very good reviews in [10, 15]

2.2. *Systems of Equations*

The application of multidimensional upwinding to a general non-linear 2D system of conservation laws

$$\frac{\partial \mathbf{w}}{\partial t} + \nabla \cdot (\mathbf{F}(\mathbf{w})) = 0, \quad \mathbf{F} = (\mathbf{f}, \mathbf{g}),$$

requires a discrete form, for the conserved variables $\mathbf{w}$, of the linearization

$$\frac{\partial \mathbf{w}}{\partial t} + (A, B)\nabla(\mathbf{w}) = 0.$$

Where, in particular, a consistent approximation for the cell residual is sought,

$$\mathbf{R}_T = (\bar{A}, \bar{B})_T \cdot \nabla \mathbf{w}_T, \tag{2.9}$$

where $\bar{A}_T, \bar{B}_T$ are discrete equivalents of the cell-averaged Jacobian matrices, calculated using the nodal values. The assumption of linear variation of $\mathbf{w}$ on each cell, enables us to write

$$\mathbf{R}_T = \frac{1}{S_T}\int_T (A, B) \cdot \nabla \mathbf{w} dS$$
$$= \frac{1}{S_T} \nabla \mathbf{w}_T \int_T (A, B) dS, \tag{2.10}$$

where discrete cell gradients and cell Jacobians can be defined in the same form as for the scalar case,

$$\nabla \mathbf{w}_T = \frac{1}{S_T}\sum_{i=1}^{3} \mathbf{w}_i \mathbf{n}_i$$

$$\bar{A} = \frac{1}{S_T}\int_T A dS$$

$$\bar{B} = \frac{1}{S_T}\int_T B dS.$$

Unfortunately, the exact evaluation of the above integrals is not practical either for the Euler or for the shallow water equations. Roe [13] suggested the introduction of a parameter set of variables for a simpler treatment of the former system. The strategy we have followed for the shallow water equations makes use of the set of primitive variables and is described in the next section.

3. THE 2D SHALLOW WATER SYSTEM

We begin this section by writing the non-homogeneous version of the system of equations in terms of the conserved variables,

$$\mathbf{U} = (h, uh, vh)^{\mathrm{T}}, \tag{3.1}$$

where h, u, and v are the depth and x and y velocities respectively, that is,

$$\frac{\partial \mathbf{U}}{\partial t} + \frac{\partial \mathbf{E}}{\partial x} + \frac{\partial \mathbf{F}}{\partial y} = \mathbf{G}, \tag{3.2}$$

where the fluxes are

$$\mathbf{E} = \begin{pmatrix} uh \\ u^2 h + \dfrac{gh^2}{2} \\ uvh \end{pmatrix}, \quad \mathbf{F} = \begin{pmatrix} vh \\ uvh \\ v^2 h + \dfrac{gh^2}{2} \end{pmatrix}.$$

The variable g is the acceleration of the gravity. The equivalent of the speed of sound in gas-dynamics, the velocity of small perturbations in still water, is the celerity c given by $c = \sqrt{gh}$, involved in the definition of the governing dimensionless Froude number $\mathrm{Fr} = \sqrt{u^2 + v^2}/c$.

The right-hand side of the system contains the sources and

sinks of momentum arising from the bed slopes and the friction losses along the two coordinate directions,

$$\mathbf{G} = (0,\ gh(S_{0x} - S_{fx}),\ gh(S_{0y} - S_{fy}))^{\mathrm{T}}.$$

The bed slopes are the spatial partial derivatives of the bottom elevation z,

$$S_{0x} = -\frac{\partial z}{\partial z}, \quad S_{0y} = -\frac{\partial z}{\partial y},$$

and the friction slopes are defined in terms of the Manning's roughness coefficient n,

$$S_{fx} = \frac{n^2 u\sqrt{u^2 + v^2}}{h^{4/3}}, \quad S_{fy} = \frac{n^2 v\sqrt{u^2 + v^2}}{h^{4/3}}.$$

The system can be rewritten in terms of the same variables but in a non-conservative form as

$$\frac{\partial \mathbf{U}}{\partial t} + A\frac{\partial \mathbf{U}}{\partial x} + B\frac{\partial \mathbf{U}}{\partial y} = 0 \tag{3.3}$$

in which only the homogeneous part has been considered. The two Jacobian matrices are

$$A = \frac{\partial \mathbf{E}}{\partial \mathbf{U}} = \begin{pmatrix} 0 & 1 & 0 \\ -u^2 + gh & 2u & 0 \\ -uv & v & u \end{pmatrix},$$

$$B = \frac{\partial \mathbf{F}}{\partial \mathbf{U}} = \begin{pmatrix} 0 & 0 & 1 \\ -uv & v & u \\ -v^2 + gh & 0 & 2v \end{pmatrix}.$$

As mentioned earlier, it will be useful later on in the paper to express the equations in terms of the primitive variables

$$\mathbf{V} = (h,\ u,\ v)^{\mathrm{T}} \tag{3.4}$$

in a non-conservative way, as

$$\frac{\partial \mathbf{V}}{\partial t} + G\frac{\partial \mathbf{V}}{\partial x} + H\frac{\partial \mathbf{V}}{\partial y} = 0, \tag{3.5}$$

where the new matrices G and H are

$$G = \begin{pmatrix} u & h & 0 \\ g & u & 0 \\ 0 & 0 & u \end{pmatrix}, \quad H = \begin{pmatrix} v & 0 & h \\ 0 & v & 0 \\ g & 0 & v \end{pmatrix}.$$

It is worth noting that the transformation matrix, M, has the form

$$M = \frac{\partial \mathbf{U}}{\partial \mathbf{V}} = \begin{pmatrix} 1 & 0 & 0 \\ u & h & 0 \\ v & 0 & h \end{pmatrix}.$$

In the conservative formulation, the fluctuation is defined as

$$\Phi_T = \int_T \mathbf{U}_t dS = -\int_T (\mathbf{E}_x + \mathbf{F}_y) dS. \tag{3.6}$$

We can use the relation between the two sets of variables to define new matrices R and S,

$$R = \frac{\partial \mathbf{E}}{\partial \mathbf{V}} = \frac{\partial \mathbf{E}}{\partial \mathbf{U}}\frac{\partial \mathbf{U}}{\partial \mathbf{V}} = AM$$

$$S = \frac{\partial \mathbf{F}}{\partial \mathbf{V}} = \frac{\partial \mathbf{F}}{\partial \mathbf{U}}\frac{\partial \mathbf{U}}{\partial \mathbf{V}} = BM$$

so that

$$\mathbf{E}_x + \mathbf{F}_y = \mathbf{E}_V \mathbf{V}_x + \mathbf{F}_V \mathbf{V}_y = R\mathbf{V}_x + S\mathbf{V}_y.$$

Provided that the variables $\mathbf{V}$ are linear over the cells T, the gradients, $\mathbf{V}_x$ and $\mathbf{V}_y$, are constant, and this would enable us to write the fluctuation as

$$\begin{aligned} \Phi_T &= -\left(\int_T (R(\mathbf{V})\mathbf{V}_x + S(\mathbf{V})\mathbf{V}_y) dS \right. \\ &= -\left(\int_T (R(\mathbf{V})dS)\mathbf{V}_x - \left(\int_T (S(\mathbf{V})dS)\mathbf{V}_y \right.\right. \\ &= -S_T[\bar{R}\mathbf{V}_x + \bar{S}\mathbf{V}_y] \end{aligned} \tag{3.7}$$

with the definitions:

$$\bar{R} = \frac{1}{S_T}\int_T R(\mathbf{V})dS, \quad \bar{S} = \frac{1}{S_T}\int_T S(\mathbf{V})dS. \tag{3.8}$$

The matrices R and S contain linear and quadratic terms in $\mathbf{V}$, which complicates integration. As mentioned in Section 2.2 it is possible to choose another variable $\mathbf{Z} = (\sqrt{h},\ u\sqrt{h},\ v\sqrt{h})$ to vary linearly over the cells according to the usual procedure for the Euler equations. Unfortunately, based on these unknowns, the corresponding matrices R and S are cubic in $\sqrt{h}$, so the argument used for the Euler equations cannot be used for the shallow water equations.

Here, we approximate $\bar{R}, \bar{S}$ by

$$\bar{R} = R(\bar{\mathbf{V}}), \quad \bar{S} = S(\bar{\mathbf{V}}), \tag{3.9}$$

where the averaged variables are simply

$$\overline{\mathbf{V}} = \begin{pmatrix} \overline{h} \\ \overline{u} \\ \overline{v} \end{pmatrix} = \frac{1}{3} \begin{pmatrix} h_1 + h_2 + h_3 \\ u_1 + u_2 + u_3 \\ v_1 + v_2 + v_3 \end{pmatrix} \tag{3.10}$$

summing over the nodal values at the vertices of the triangle T. Note that with this definition of $\overline{R}, \overline{S}$ we are only approximating Eq. (3.8), unlike in the Euler equations where an exact representation of the integral is obtained. As a consequence, we lose conservation in the numerical evaluation of the fluctuation.

Now we have

$$(\Phi_T \approx) - S_T(\overline{\mathbf{E}}_x + \overline{\mathbf{F}}_y) = -S_T(\overline{A}\,\overline{\mathbf{U}}_x + \overline{B}\,\overline{\mathbf{U}}_y). \tag{3.11}$$

From (3.7) it is easy to identify

$$\begin{aligned} \overline{\mathbf{E}}_x &= \overline{R}\mathbf{V}_x \\ \overline{\mathbf{F}}_y &= \overline{S}\mathbf{V}_y. \end{aligned} \tag{3.12}$$

Moreover, we can use the change of variables to define

$$S_T\overline{\mathbf{U}}_x = \int_T \mathbf{U}_x dS = \int_T M(\mathbf{V})\mathbf{V}_x dS = S_T M(\overline{\mathbf{V}})\mathbf{V}_x$$

so that

$$\overline{\mathbf{U}}_x = M(\overline{\mathbf{V}})\mathbf{V}_x \tag{3.13}$$

$$\mathbf{V}_x = M^{-1}(\overline{\mathbf{V}})\overline{\mathbf{U}}_x \tag{3.14}$$

with similar expressions for $\overline{\mathbf{U}}_y$ and $\mathbf{V}_y$. This can be used to rewrite the fluctuation in terms of suitable averages of the conserved variables,

$$\begin{aligned} (\Phi_T \approx) &-[\overline{R}M^{-1}(\overline{\mathbf{V}})\overline{\mathbf{U}}_x + \overline{S}M^{-1}(\overline{\mathbf{V}})\overline{\mathbf{U}}_y]S_T \\ &= -[\overline{A}\,\overline{\mathbf{U}}_x + \overline{B}\,\overline{\mathbf{U}}_y]S_T, \end{aligned} \tag{3.15}$$

which allows the identification of $\overline{A}$ and $\overline{B}$.

$$\begin{aligned} \overline{A} &= R(\overline{\mathbf{V}})M^{-1}(\overline{\mathbf{V}}) = \left.\frac{\partial \mathbf{E}}{\partial \mathbf{V}}\right|_{\overline{V}} \left.\frac{\partial \mathbf{V}}{\partial \mathbf{U}}\right|_{\overline{V}} = \left.\frac{\partial \mathbf{E}}{\partial \mathbf{U}}\right|_{\overline{V}} = A(\overline{V}) \\ \overline{B} &= S(\overline{\mathbf{V}})M^{-1}(\overline{\mathbf{V}}) = \left.\frac{\partial \mathbf{F}}{\partial \mathbf{V}}\right|_{\overline{V}} \left.\frac{\partial \mathbf{V}}{\partial \mathbf{U}}\right|_{\overline{V}} = \left.\frac{\partial \mathbf{F}}{\partial \mathbf{U}}\right|_{\overline{V}} = B(\overline{V}). \end{aligned} \tag{3.16}$$

The next thing we have to do is to compute the residuals R_T or the fluctuations and distribute them to the vertices of every cell by means of an advection scheme. Recalling that at the beginning of the time step we have the values of the conserved variables at the vertices of the triangular mesh, the steps to follow are: to compute the primitive variables $\mathbf{V}$ from the known $\mathbf{U}$, work out the gradients $\nabla\mathbf{V} = (\mathbf{V}_x, \mathbf{V}_y)$ within each triangle, and decompose the residual into parts that can be explained as due to the passage of a wave. The latter step will require a description of wave models.

4. WAVE MODELS

Consider the linearized system of equations written in primitive variables

$$\frac{\partial \mathbf{V}}{\partial t} + \overline{G}\frac{\partial \mathbf{V}}{\partial x} + \overline{H}\frac{\partial \mathbf{V}}{\partial y} = 0. \tag{4.1}$$

A simple wave solution can be found, as in Roe [11,12], in the form

$$\mathbf{V} = \mathbf{V}(\xi) \quad \text{with } \xi = \mathbf{x}.\mathbf{n}_\theta - \lambda_\theta t,$$

where $\mathbf{n}_\theta = (\cos\theta, \sin\theta)$ gives the direction of propagation and λ_θ the speed of the wave. If we note that

$$\frac{\partial \mathbf{V}}{\partial t} = -\lambda_\theta \frac{d\mathbf{V}}{d\xi}$$

and

$$\nabla\mathbf{V} = \frac{d\mathbf{V}}{\xi}\mathbf{n}_\theta,$$

it follows from (4.1) that

$$-\lambda_\theta \frac{d\mathbf{V}}{d\xi} + (\overline{G}\cos\theta + \overline{H}\sin\theta)\frac{d\mathbf{V}}{d\xi} = 0$$

which means that $d\mathbf{V}/d\xi$ are the right eigenvectors of the matrix

$$M^* = \overline{G}\cos\theta + \overline{H}\sin\theta \tag{4.2}$$

and λ_θ are the corresponding eigenvalues.

It is then possible to express the gradient as the sum

$$\nabla\mathbf{V} = \sum_{k=1}^{n} \alpha^k \mathbf{r}^k \mathbf{n}^k, \tag{4.3}$$

that is,

$$\mathbf{V}_x = \sum_{k=1}^{n} \alpha^k \mathbf{r}^k \cos\theta^k$$

$$\mathbf{V}_y = \sum_{k=1}^{n} \alpha^k \mathbf{r}^k \sin\theta^k.$$

The vectors $\mathbf{r}^k$ are the right eigenvectors of the matrix M^*:

$$\mathbf{r}^1 = \begin{pmatrix} 1 \\ \frac{g}{c}\cos\theta \\ \frac{g}{c}\sin\theta \end{pmatrix}, \quad \mathbf{r}^2 = \begin{pmatrix} 1 \\ -\frac{g}{c}\cos\theta \\ -\frac{g}{c}\sin\theta \end{pmatrix}, \quad \mathbf{r}^3 = \begin{pmatrix} 0 \\ -\sin\theta \\ \cos\theta \end{pmatrix}. \tag{4.4}$$

The variables α^k represent weighting coefficients of the sum and θ^k are the different angles of each wave.

The connection expressed in (3.13) between the gradient of the primitive variables and that of the averaged conservative variables can be used to develop the latter as

$$\overline{\mathbf{U}}_x = \sum_{k=1}^{n} \alpha^k \mathbf{r}_c^k \cos\theta^k$$

$$\overline{\mathbf{U}}_y = \sum_{k=1}^{n} \alpha^k \mathbf{r}_c^k \sin\theta^k,$$

where, now, $\mathbf{r}_c^k$ represent the right eigenvectors of the matrix

$$M_c^* = \overline{A}\cos\theta + \overline{B}\sin\theta$$

and can be worked out through $\mathbf{r}_c^k = M(\overline{\mathbf{V}})\mathbf{r}^k$. It is worth noting here that the two matrices M^* and M_c^* share the unique set of eigenvalues, λ^k,

$$\begin{aligned} \lambda^1 &= \overline{u}\cos\theta + \overline{v}\sin\theta + c \\ \lambda^2 &= \overline{u}\cos\theta + \overline{v}\sin\theta - c \\ \lambda^3 &= \overline{u}\cos\theta + \overline{v}\sin\theta. \end{aligned} \tag{4.5}$$

The residual then can be split into a sum of waves

$$\begin{aligned} R_T &= \overline{A}\,\overline{\mathbf{U}}_x + \overline{B}\,\overline{\mathbf{U}}_y \\ &= \overline{A}\sum_{k=1}^{n} \alpha^k \mathbf{r}_c^k \cos\theta^k + \overline{\mathbf{B}}\sum_{k=1}^{n} \alpha^k \mathbf{r}_c^k \sin\theta^k \\ &= \sum_{k=1}^{n} \alpha^k [\overline{A}\cos\theta^k + \overline{B}\sin\theta^k]\mathbf{r}_c^k \\ &= \sum_{k=1}^{n} \alpha^k \lambda^k \mathbf{r}_c^k. \end{aligned} \tag{4.6}$$

We next describe two of the several wave models proposed in the literature to accomplish the above decomposition.

4.1. *Roe's Wave Models*

The wave decomposition of the gradient of the primitive variables, namely,

$$\nabla\mathbf{V} = \sum_{k=1}^{n} \alpha^k \mathbf{r}^k \mathbf{n}^k, \tag{4.7}$$

represents a system of six equations in the shallow water case, where we have two spatial derivatives for each of the three variables. Therefore, it allows for six unknowns. These must correspond to either the coefficients or the angles of a propagation of suitable choices of waves whose advection will represent the total fluctuation.

Following Roe's suggestions for the treatment of the Euler equations [11], the splitting can be made into four orthogonal acoustic waves, labelled by their strengths (coefficients) and one angle θ which determines the four directions, defined by

$$(\alpha_1, \theta), (\alpha_2, \theta + \pi), \left(\alpha^3, \theta + \frac{\pi}{2}\right), \left(\alpha^4, \theta + \frac{3\pi}{2}\right),$$

as well as one shear wave (β, ϕ) of strength β at an angle ϕ. The six unknowns are then α_1, α_2, α_3, α_4, β, and θ. The value of the angle ϕ, in Roe's model D, can be defined in terms of the solution as

$$\phi = \theta - \frac{\pi}{4}\,\mathrm{sign}(\beta).$$

Making use of the equivalences of the basic trigonometric functions to those of the first quadrant of the unit radius circle, the system (4.7) can be explicitly written as

$$\begin{aligned} \frac{\partial h}{\partial x} &= \alpha_1\cos\theta - \alpha_2\cos\theta - \alpha_3\sin\theta + \alpha_4\sin\theta \\ \frac{\partial h}{\partial y} &= \alpha_1\sin\theta - \alpha_2\sin\theta + \alpha_3\cos\theta - \alpha_4\cos\theta \\ \frac{\partial u}{\partial x} &= \frac{g}{c}[\alpha_1\cos^2\theta + \alpha_2\cos^2\theta + \alpha_3\sin^2\theta + \alpha_4\sin^2\theta] \\ &\quad - \beta\sin\phi\cos\phi \\ \frac{\partial u}{\partial y} &= \frac{g}{c}[\alpha_1\sin\theta\cos\theta + \alpha_2\sin\theta\cos\theta - \alpha_3\sin\theta\cos\theta \\ &\quad - \alpha_4\sin\theta\cos\theta] - \beta\sin^2\phi \\ \frac{\partial v}{\partial x} &= \frac{g}{c}[\alpha_1\sin\theta\cos\theta + \alpha_2\sin\theta\cos\theta - \alpha_3\sin\theta\cos\theta \\ &\quad - \alpha_4\sin\theta\cos\theta] + \beta\cos^2\phi \\ \frac{\partial v}{\partial y} &= \frac{g}{c}[\alpha_1\sin^2\theta + \alpha_2\sin^2\theta + \alpha_3\cos^2\theta + \alpha_4\cos^2\theta] \\ &\quad + \beta\sin\phi\cos\phi. \end{aligned} \tag{4.8}$$

The solution of the above algebraic system is easily found giving, for the coefficient of the shear wave,

$$\beta = |\beta|\,\mathrm{sign}(\beta) = v_x - u_y. \tag{4.9}$$

The identities

$$\beta(\cos^2\phi - \sin^2\phi) = |\beta| \sin 2\theta$$
$$2\beta \sin\phi \cos\phi = -|\beta| \cos 2\theta$$

are helpful in combining the derivatives as

$$u_y + v_x = \left[\frac{g}{c}(\alpha_1 + \alpha_2 - \alpha_3 - \alpha_4) + |\beta|\right] \sin 2\theta$$
$$u_x - v_y = \left[\frac{g}{c}(\alpha_1 + \alpha_2 - \alpha_3 - \alpha_4) + |\beta|\right] \cos 2\theta$$

so that

$$\tan 2\theta = \frac{u_y + v_x}{u_x - v_y}. \tag{4.10}$$

Further manipulations of the derivatives lead us to

$$u_x \cos^2\theta - v_y \sin^2\theta = \left[\frac{g}{c}(\alpha_1 + \alpha_2) + \frac{1}{2}|\beta|\right] \cos 2\theta$$

and

$$h_x \cos\theta + h_y \sin\theta = \alpha_1 - \alpha_2,$$

hence, to the values

$$\alpha_1 = \frac{1}{2}\left[h_x \cos\theta + h_y \sin\theta + \frac{c}{g}\left(\frac{u_x \cos^2\theta - v_y \sin^2\theta}{\cos 2\theta} - \frac{1}{2}|\beta|\right)\right] \tag{4.11}$$

$$\alpha_2 = \frac{1}{2}\left[-(h_x \cos\theta + h_y \sin\theta) + \frac{c}{g}\left(\frac{u_x \cos^2\theta - v_y \sin^2\theta}{\cos 2\theta} - \frac{1}{2}|\beta|\right)\right]. \tag{4.12}$$

A similar procedure gives

$$\alpha_3 = \frac{1}{2}\left[h_y \cos\theta - h_x \sin\theta + \frac{c}{g}\left(\frac{v_y \cos^2\theta - u_x \sin^2\theta}{\cos 2\theta} + \frac{1}{2}|\beta|\right)\right] \tag{4.13}$$

$$\alpha_4 = \frac{1}{2}\left[-(h_y \cos\theta - h_x \sin\theta) + \frac{c}{g}\left(\frac{v_y \cos^2\theta - u_x \sin^2\theta}{\cos 2\theta} + \frac{1}{2}|\beta|\right)\right]. \tag{4.14}$$

In order to distribute the residuals associated with the individual waves in this case, we used the advection speeds suggested by Roe in [11], $\mathbf{u} \pm c\mathbf{n}_\theta$ for the acoustic waves and $\mathbf{u}$ for the shear wave.

4.2. *Rudgyard's Wave Models*

These are mainly based on the idea of obtaining the six waves by choosing two, in principle, arbitrary propagation angles, θ_1 and θ_2, and performing a decomposition of the gradient,

$$\nabla \mathbf{V} = \sum_{k=1}^{3} \alpha_{\theta 1}^k \mathbf{r}_{\theta 1}^k \mathbf{n}_{\theta 1} + \sum_{k=1}^{3} \alpha_{\theta 2}^k \mathbf{r}_{\theta 2}^k \mathbf{n}_{\theta 2} \tag{4.15}$$

which contains six free parameters, the six α coefficients. The vectors $\mathbf{n}_\theta = (\cos\theta, \sin\theta)$ are again the unit vectors in the directions θ, and $\mathbf{r}_\theta^k$ are the right eigenvectors of the matrix M^* for each value of θ. In order to solve for the unknowns, use is also made of the left eigenvectors of that matrix

$$\mathbf{l}_\theta^1 = \begin{pmatrix} \frac{1}{2} \\ \frac{c}{2g}\cos\theta \\ \frac{c}{2g}\sin\theta \end{pmatrix}, \quad \mathbf{l}_\theta^2 = \begin{pmatrix} \frac{1}{2} \\ -\frac{c}{2g}\cos\theta \\ -\frac{c}{2g}\sin\theta \end{pmatrix}, \quad \mathbf{l}_\theta^3 = \begin{pmatrix} 0 \\ -\sin\theta \\ \cos\theta \end{pmatrix} \tag{4.16}$$

and of the unit vector normal to $\mathbf{n}_\theta$,

$$\mathbf{s}_\theta = (-\sin\theta, \cos\theta).$$

Multiplication of (4.16) on the left by $\mathbf{l}_{\theta 1}^i$ and the left projection over $\mathbf{s}_{\theta 2}$ gives

$$\mathbf{s}_{\theta 2} \cdot (\mathbf{l}_{\theta 1}^i \cdot \nabla \mathbf{V}) = \alpha_{\theta 1}^i (\mathbf{s}_{\theta 2} \cdot \mathbf{n}_{\theta 1}), \tag{4.17}$$

where the property $\mathbf{l}_\theta^i \cdot \mathbf{r}_\theta^j = \delta_{ij}$ and the orthogonality between vectors $\mathbf{s}$ and $\mathbf{n}$ have been used.

From (4.17), we obtain

$$\alpha_{\theta 1}^i = -\frac{\mathbf{s}_{\theta 2} \cdot (\mathbf{l}_{\theta 1}^i \cdot \nabla \mathbf{V})}{\sin(\theta_2 - \theta_1)}. \tag{4.18}$$

In case the above notation may be rather obscure, the vector products contained can be developed as

$$\alpha_{\theta 1}^i = -\frac{1}{\sin(\theta_2 - \theta_1)} \left[(-\sin\theta_2, \cos\theta_2)\frac{1}{2}\begin{pmatrix} h_x + \frac{c}{g}\cos\theta_1 u_x + \frac{c}{g}\sin\theta_1 v_x \\ h_y + \frac{c}{g}\cos\theta_1 u_y + \frac{c}{g}\sin\theta_1 v_y \end{pmatrix}\right].$$

In that way, the six unknowns of the problem are given by

$$\alpha^k_{\theta 1} = -\frac{\mathbf{s}_{\theta 2} \cdot (\mathbf{l}^k_{\theta 1} \cdot \nabla \mathbf{V})}{\sin(\theta_2 - \theta_1)}, \quad \alpha^k_{\theta 2} = \frac{\mathbf{s}_{\theta 1} \cdot (\mathbf{l}^k_{\theta 2} \cdot \nabla \mathbf{V})}{\sin(\theta_2 - \theta_1)}. \quad (4.19)$$

As an illustration, in the particular case of choosing as propagation angles, $\theta_1 = 0$, $\theta_2 = \pi/2$,

$$\alpha^1_{\theta 1} = \frac{1}{2}\left(h_x + \frac{c}{g}u_x\right)$$

$$\alpha^2_{\theta 1} = \frac{1}{2}\left(h_x - \frac{c}{g}u_x\right)$$

$$\alpha^3_{\theta 1} = v_x$$

$$\alpha^1_{\theta 2} = \frac{1}{2}\left(h_y + \frac{c}{g}v_y\right)$$

$$\alpha^2_{\theta 2} = \frac{1}{2}\left(h_y - \frac{c}{g}v_y\right)$$

$$\alpha^3_{\theta 2} = -u_y.$$

Following [14], the residuals of the waves from this model were advected with the speeds

$$\lambda^k_{\theta 1} = -\frac{\lambda^k_{\theta 1}\mathbf{s}_{\theta 2}}{\sin(\theta_2 - \theta_1)}, \quad \lambda^k_{\theta 2} = \frac{\lambda^k_{\theta 2}\mathbf{s}_{\theta 1}}{\sin(\theta_2 - \theta_1)}.$$

4.3. *Mach-Angle Splitting*

One of the options proposed within Rudgyard's wave models [14] is the particular choice of the angles that satisfy the equation

$$\mathbf{u} \cdot \mathbf{n} - c = 0, \quad (4.20)$$

that is, those angles that make the velocity of one of the acoustic waves vanish. They are obtained from algebraic manipulation of (4.20) and can be expressed as

$$\theta_1 = \arctan\left(\frac{v + u\sqrt{(M^2 - 1)}}{u - v\sqrt{(M^2 - 1)}}\right)$$
$$\theta_2 = \arctan\left(\frac{v - u\sqrt{(M^2 - 1)}}{u + v\sqrt{(M^2 - 1)}}\right) \quad (4.21)$$

with $M^2 = (u^2 + v^2)/c^2$ representing the Froude number in this case. This technique gives very good results in gasdynamics problems for supersonic flows but is not directly applicable to the subsonic case. It can nevertheless be adapted for subsonic (subcritical in our case) flows by replacing $M^2 - 1$ with $\max(|M^2 - 1|, \varepsilon)$, the tolerance ε taking a typical value of 0.1.

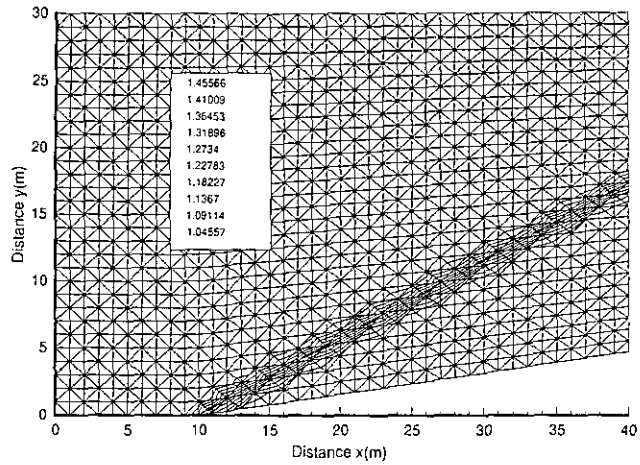

FIG. 1. Map of level lines from the numerical result obtained in the 2400 elements grid. The continuous line leaving the domain by the downstream side represents the exact position of the steady shock.

5. NUMERICAL RESULTS

The treatment of the solution at the points on the boundaries of the domain has been kept as close as possible to the theory of characteristics in 2D. In all cases, the number of physical conditions to be imposed has been determined by this theory. This number is defined [6] by the signs of the eigenvalues λ of the matrix

$$K = An_x + Bn_y, \quad (5.1)$$

where the boundary normal vector $\mathbf{n}$ is the unit vector pointing into the domain. The eigenvalues are associated with the celerities of the waves. Hence, when λ is positive, the information travels along the normal, into the domain. When it is negative,

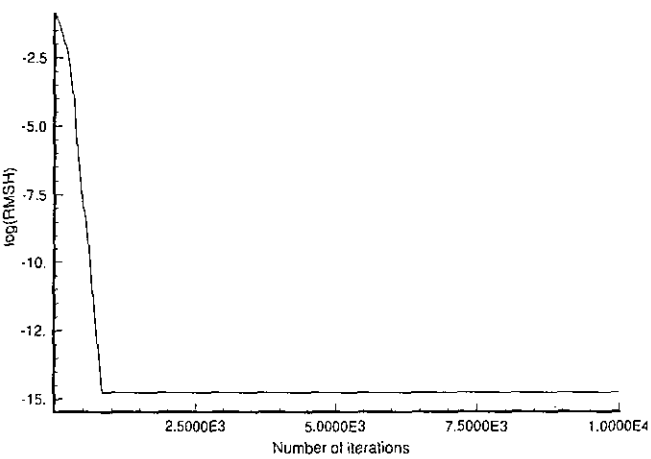

FIG. 2. Convergence to the steady state. Plot of the logarithm of the root mean square of the nodal residuals of the conservation of mass equation versus number of iterations performed.

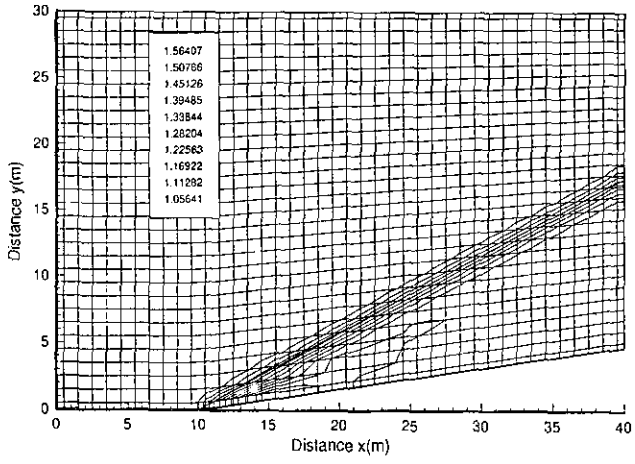

FIG. 3. Map of level lines from the numerical result obtained with a finite volumes TVD scheme in a (42 × 7) quadrilateral cell.

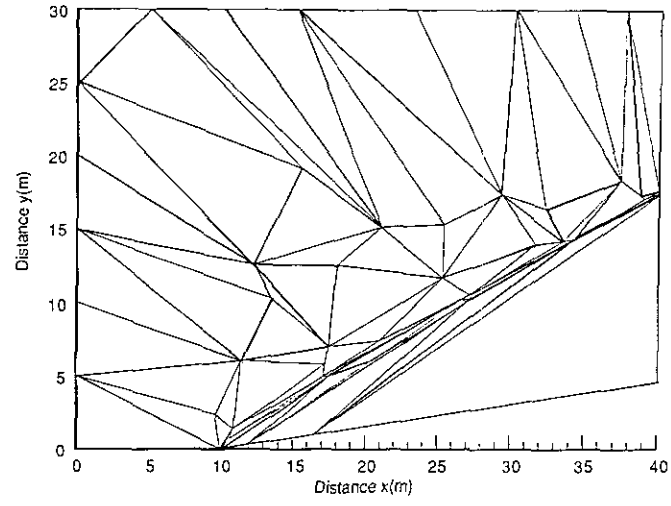

FIG. 5. Above: 96 elements distorted grid used for the oblique jump test case.

the information goes against the normal, that is out of the domain. The subcritical cases are the most illustrative, having, at a subcritical inlet for instance, $\mathbf{u} \cdot \mathbf{n} > 0$ and $\mathbf{u} \cdot \mathbf{n} < c$, so that,

$$\lambda_1 = \mathbf{u} \cdot \mathbf{n} < 0$$

$$\lambda_2 = \mathbf{u} \cdot \mathbf{n} + c > 0$$

$$\lambda_3 = \mathbf{u} \cdot \mathbf{n} - c < 0.$$

This means that there are two waves from outside and therefore, two boundary conditions have to be imposed. The wave from inside produces a numerical boundary condition. In an analogous manner, the case of a subcritical outlet requires only one imposed external boundary condition. The information that travels from inside the domain is determined by the compatibility relations which can be written for arbitrary propagation directions from the 2D theory of characteristics. These have been simplified by assuming that the derivatives along the direction tangential to the boundary are negligible. In the case of a material wall boundary, a zero normal velocity is imposed and the depth as well as tangential velocity are calculated from the compatibility conditions.

For the interior points we used the non-linear PSI advection algorithm [10] for all the test cases following but obtained very similar results with the other advection schemes. As for the wave model, the calculations correspond to Rudgyard's decomposition having been found more robust, in general, than the one corresponding to Roe's model D.

5.1. *Oblique Hydraulic Jump*

With numerical schemes it is highly desirable to be able to check their predictions against suitable test problems, prefer-

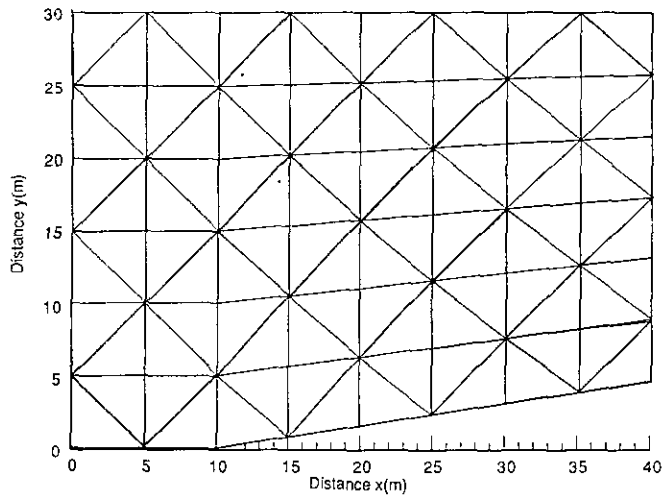

FIG. 4. 96 elements initial grid used for the oblique jump test case.

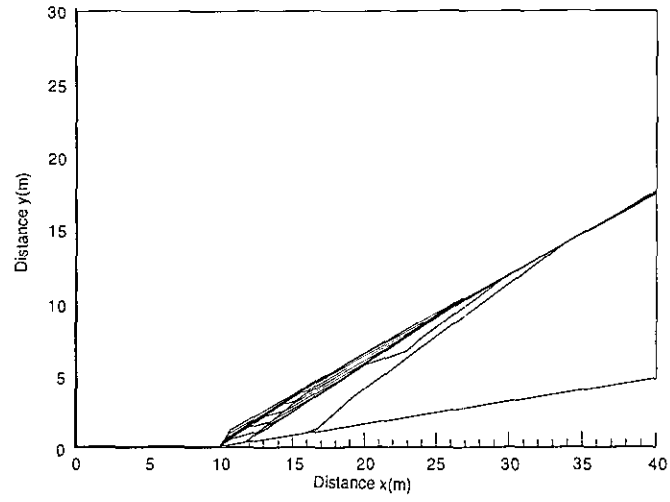

FIG. 6. Map of level lines from the numerical result obtained in the 96 elements distorted grid.

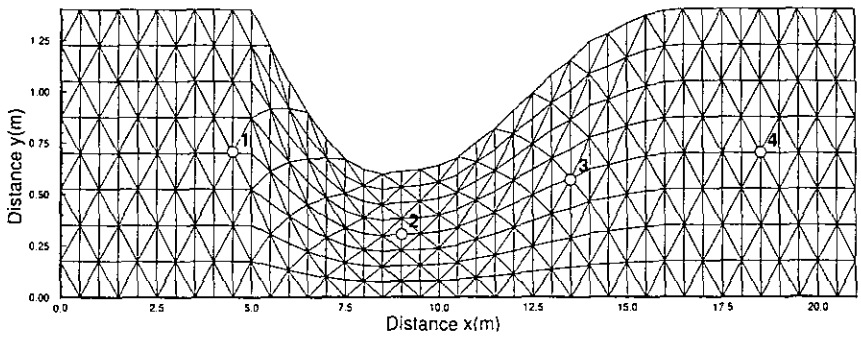

FIG. 7. Unsteady flow through a converging diverging channel. Grid, geometry and points of measurement.

ably ones for which an exact solution is available. Such is the case for the example below, computed by a finite volume method by Alcrudo and Garcia-Navarro [1], in which an oblique hydraulic jump is induced by means of the interaction between a supercritical flow and a wall at an angle θ. The equation for the angle formed by the shock wave is defined by

$$\sin\beta = \frac{1}{\mathrm{Fr}_1}\sqrt{(h_2/2h_1)(h_2/h_1 + 1)}. \tag{5.2}$$

A 2400-element triangular mesh, shown in Fig. 1, was used to reproduce the discontinuous flow in a case where $\theta = 8.95°$. The initial conditions were $h = 1$ m, $u = 8.57$ m/s and $v = 0$ m/s, that is, a uniform supercritical flow with Fr = 2.74. Supercritical flow boundary conditions were applied both upstream and downstream. This means that all the variables were specified in the former and all of them updated from interior points in the latter.

The exact solution corresponding to the upstream flow and geometry imposed was calculated. The predicted values were $h_2 = 1.5$ m, $|u_2| = 7.9556$, $\mathrm{Fr}_2 = 2.075$ for the downstream variables, and $\beta = 30°$ for the angle of the jump connecting them to the given upstream conditions. As can be seen in Fig. 1 as well, the agreement of the numerical results with the correct solution, represented by a continuous line leaving the domain, was good. The angle formed by the well-defined oblique hydraulic jump is closely reproduced as well as the values of the flow variables on both sides of it ($h_2 = 1.5049$ m, $|u_2| = 7.9419$, $\mathrm{Fr}_2 = 2.068$) and a discontinuous water surface devoid of oscillations is obtained.

For the convergence to the steady state, a local time stepping was used with a CFL = 0.9 and Rudgyard's Mach-angle splitting method was found to give the best convergence rate shown

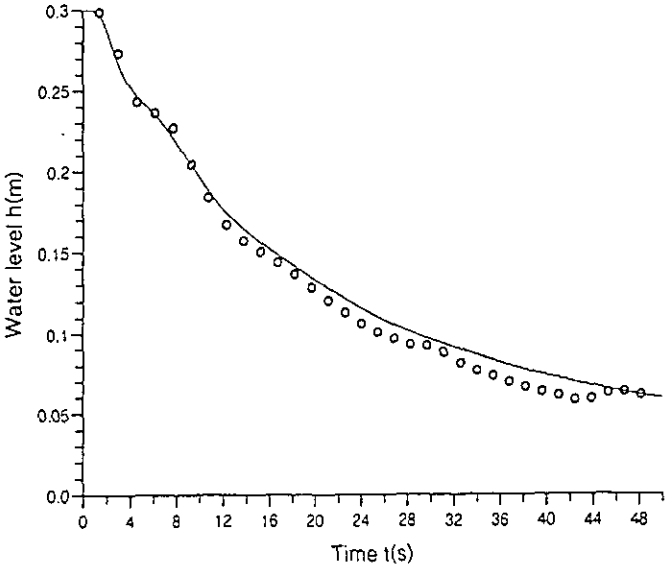

FIG. 8. Test case $S_{0x} = 0.0$, $h_1 = 0.3$ m, $h_2 = 0.053$ m. Continuous line: Predicted values. Circles: Measured values. Section 1. Multidimensional upwinding scheme.

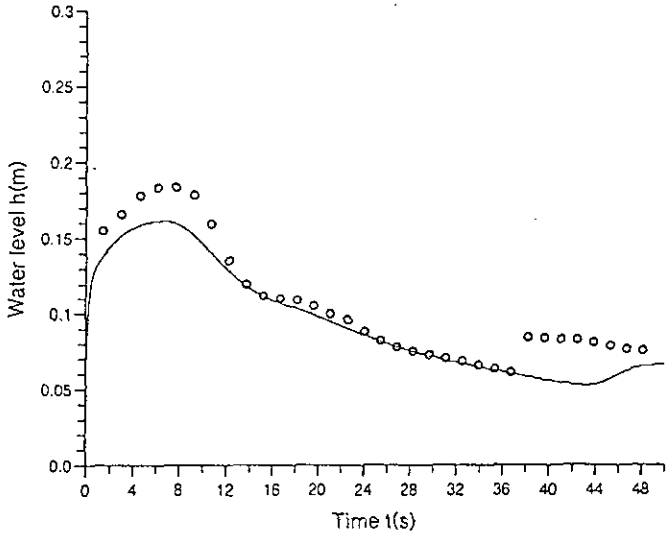

FIG. 9. Test case $S_{0x} = 0.0$, $h_1 = 0.3$ m, $h_2 = 0.053$ m. Continuous line: Predicted values. Circles: Measured values. Section 2. Multidimensional upwinding scheme.

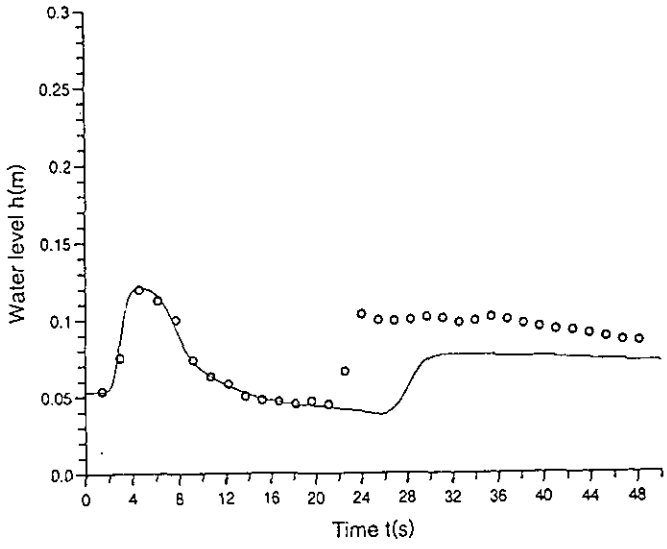

FIG. 10. Test case $S_{0x} = 0.0$, $h_1 = 0.3$ m, $h_2 = 0.053$ m. Continuous line: Predicted values. Circles: Measured values. Section 3. Multidimensional upwinding scheme.

by Fig. 2. The same degree of accuracy is achieved with both fluctuation splitting and the TVD in finite volume method reported in [1], but at a higher computational cost in the case of the former technique (a factor of about 5). The results obtained with the TVD method in a quadrilateral grid can be seen in Fig. 3. A strategy of cell movement proposed by Baines [5] can be nevertheless exploited for the unstructured grid in order to overcome this difficulty. The possibility of using an algorithm capable of making the cells migrate towards the regions of steeper gradients allows the reduction of the total number of

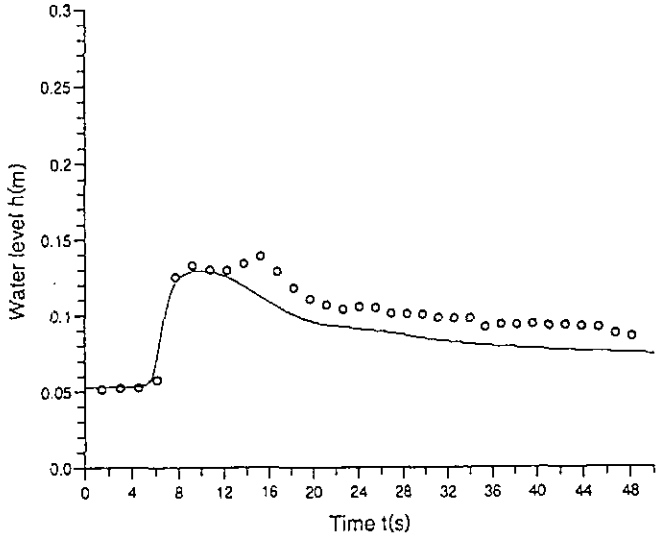

FIG. 11. Test case $S_{0x} = 0.0$, $h_1 = 0.3$ m, $h_2 = 0.053$ m. Continuous line: Predicted values. Circles: Measured values. Section 4. Multidimensional upwinding scheme.

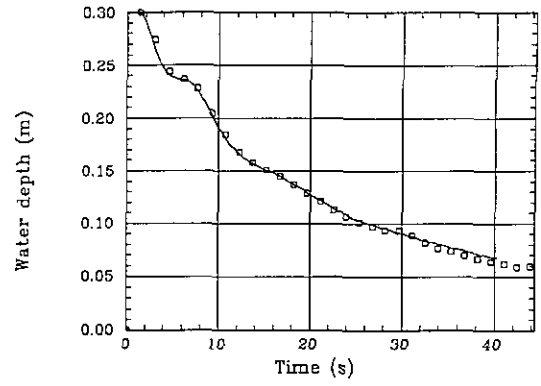

FIG. 12. Test case $S_{0x} = 0.0$, $h_1 = 0.3$ m, $h_2 = 0.053$ m. Continuous line: Predicted values. Circles: Measured values. Section 1. TVD scheme.

cells. A preliminary, but encouraging, result is displayed in Figs. 4-6. Figure 4 shows the 96 element grid that has been automatically rearranged according to the evolution towards the steady state of the flow, Fig. 5. The accuracy of the result displayed in Fig. 6 is superior and the computational time has been reduced to half of that used by the TVD method.

5.2. *Unsteady Flow in a Converging–Diverging Sloping Channel*

In order to test the performance of the multidimensional upwinding when including source terms in the system of equations, a simulation of a dambreak wave in a 2D laboratory experiment, as reported in [3], is presented. At the same time, and unlike in the case of the Euler equations, most practical problems involving the shallow water equations are time-dependent, so this problem also tests the temporal accuracy of the method. The treatment of the source terms was done simply by calculation of the functions at the vertices of every cell, including these values in the updating at every time level, that is, in a pointwise manner. A better approach could be an integration of the source terms over the triangle and further

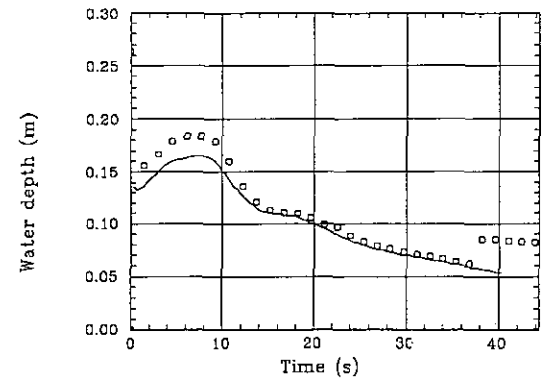

FIG. 13. Test case $S_{0x} = 0.0$, $h_1 = 0.3$ m, $h_2 = 0.053$ m. Continuous line: Predicted values. Circles: Measured values. Section 2. TVD scheme.

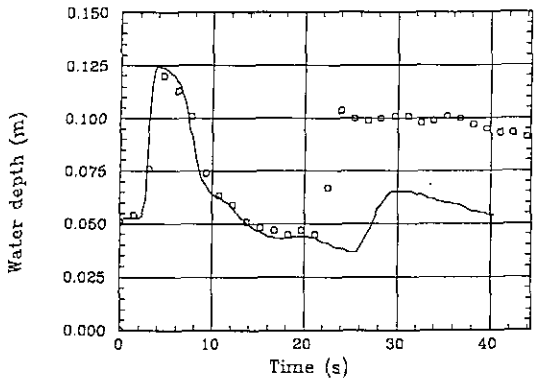

FIG. 14. Test case $S_{0x} = 0.0$, $h_1 = 0.3$ m, $h_2 = 0.053$ m. Continuous line: Predicted values. Circles: Measured values. Section 3. TVD scheme.

distribution to the nodes. Certainly, this would improve conservation as long as the integration is done exactly, which can become expensive because the source terms are non-linear in h, u and v. Treating the source terms pointwise is a sensible thing to try first due to its simplicity.

The channel is 21 m long and 1.4 m wide at it widest part. It has a uniform bottom slope S_{0x} along the direction of the main flow. The roughness of the surface (smooth steel-glass) is represented by a uniform Manning's coefficient $n = 0.012$. Measured data of the water levels as a function of time were available at several positions along the centreline of the flume and they were located over nodal points of the computational grid chosen. The validation of the method was done on a 672-element triangular grid. The measurement points used to validate the numerical results, as well as the geometry of the channel are shown over the grid in Fig. 7. The uncertainty of the measurements is not available in [3] but the supplied data contain water level variations in time with a precision of one-tenth of a millimeter, which makes sensible the estimation of an error band of 1 mm or less.

A dam is placed in the constriction, at $x = 8.5$ m from the origin, where the width is 0.6 m. The discontinuous initial conditions consist of a horizontal surface level on the upstream side, with a depth of 0.3 m just behind the dam, and a uniform water depth downstream. All velocities are initially set equal to zero. Some authors impose Ritter's initial conditions at the damsite. This is an acceptable strategy for certain numerical schemes not able to deal with strong discontinuities at $t = 0$. The lateral and upstream boundaries are treated as closed walls. The downstream side was treated as a supercritical boundary in the sense of not applying any particular external boundary

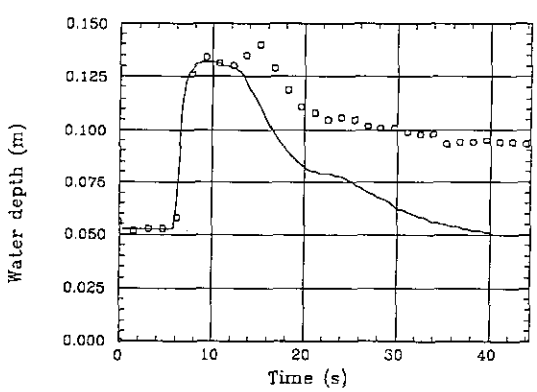

FIG. 15. Test case $S_{0x} = 0.0$, $h_1 = 0.3$ m, $h_2 = 0.053$ m. Continuous line: Predicted values. Circles: Measured values. Section 4. TVD scheme.

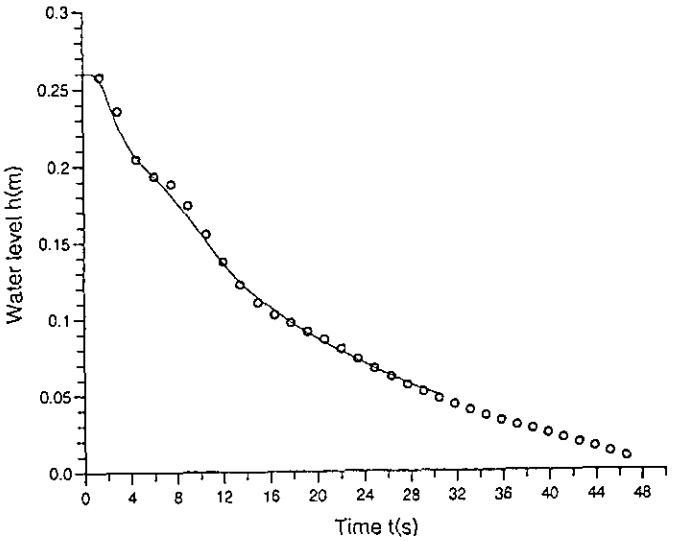

FIG. 16. Test case $S_{0x} = 0.01$, $h_1 = 0.3$ m, $h_2 = 0.0$ m. Continuous line: Predicted values. Circles: Measured values. Section 1. Multidimensional upwinding scheme.

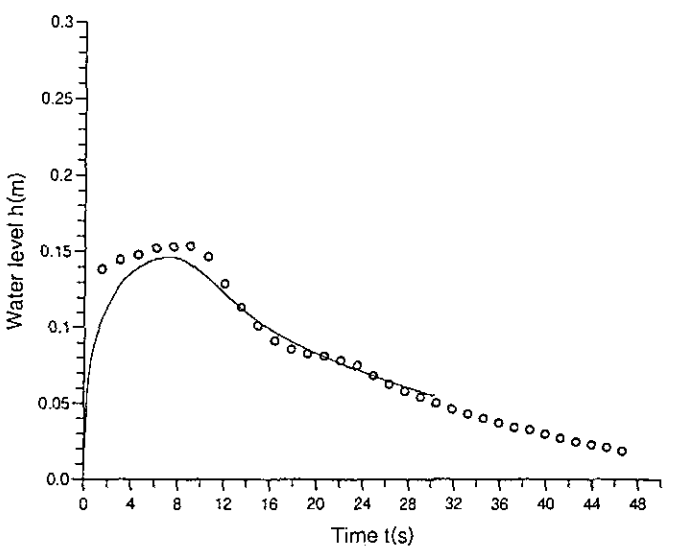

FIG. 17. Test case $S_{0x} = 0.01$, $h_1 = 0.3$ m, $h_2 = 0.0$ m. Continuous line: Predicted values. Circles: Measured values. Section 2. Multidimensional upwinding scheme.

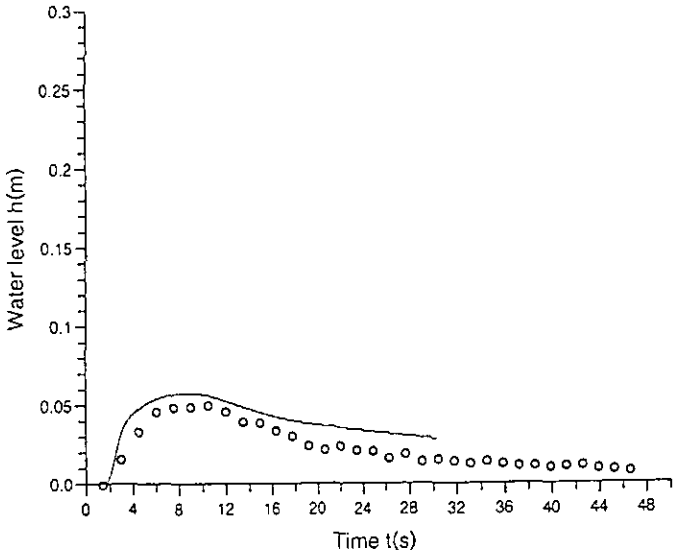

FIG. 18. Test case $S_{0x} = 0.01$, $h_1 = 0.3$ m, $h_2 = 0.0$ m. Continuous line: Predicted values. Circles: Measured values. Section 3. Multidimensional upwinding scheme.

condition but calculating the values of the variables from the normal updating at the vertices.

The case of dambreak flood wave propagation over an initial water depth $h_2 = 0.053$ m and zero bottom slope is displayed in Figs. 8–11. The results from the calculation are plotted as a solid line and the circles represent the measured data. The solid lines follow closely the experimental results. Apart from downstream boundary effects, the wave front celerity and intensity are well reproduced by the model, as indicated by the rising

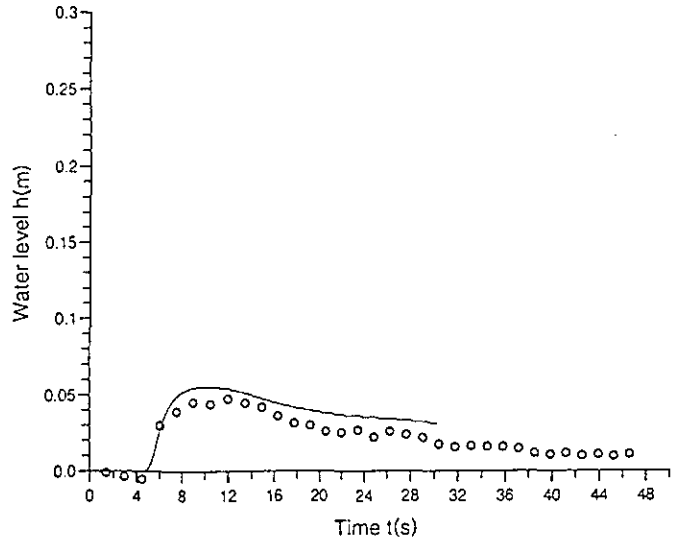

FIG. 19. Test case $S_{0x} = 0.01$, $h_1 = 0.3$ m, $h_2 = 0.0$ m. Continuous line: Predicted values. Circles: Measured values. Section 4. Multidimensional upwinding scheme.

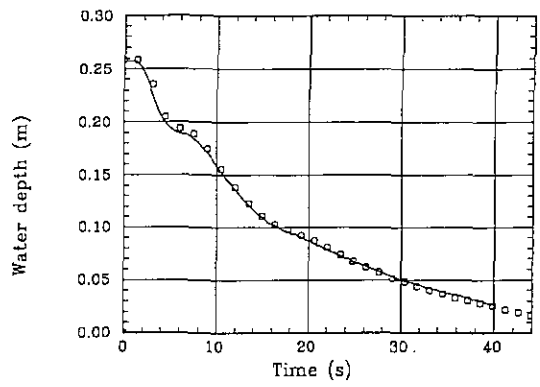

FIG. 20. Test case $S_{0x} = 0.01$, $h_1 = 0.3$ m, $h_2 = 0.0$ m. Continuous line: Predicted values. Circles: Measured values. Section 1. TVD scheme.

parts of the curve in Figs. 10, 11. A weir was placed downstream in the experimental setup in order to keep constant the initial downstream water level. The interaction of this weir with the flood wave originated a reflected front which can be seen as an abrupt increase in water level in Figs. 9–11. The good agreement between calculation and experimental data deteriorates when the moving reflected wave is met, rendering the plots meaningless from that moment. The use of a boundary condition different from the weir equation is responsible for this circumstance which is independent of the scheme used in the interior and it also happens with other numerical solutions, as reported in [9] and shown in Figs. 12–15.

Dry bed initial conditions downstream of the dam corresponding to a bottom slope $S_{0x} = 0.01$ were also tried. Zero initial depth was simulated by a value of 10^{-6} m. The set of results is plotted in Figs. 16–19. The overall quality of the results is as good as those obtained with a high order finite volume method [3, 9] as Figs. 20–23 show.

The calculation of the results presented was performed with a global time-stepping in order to be able to compare with the experimental data available. The CFL used was 0.8.

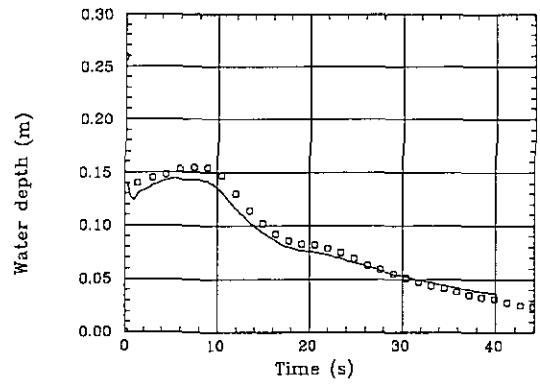

FIG. 21. Test case $S_{0x} = 0.01$, $h_1 = 0.3$ m, $h_2 = 0.0$ m. Continuous line: Predicted values. Circles: Measured values. Section 2. TVD scheme.

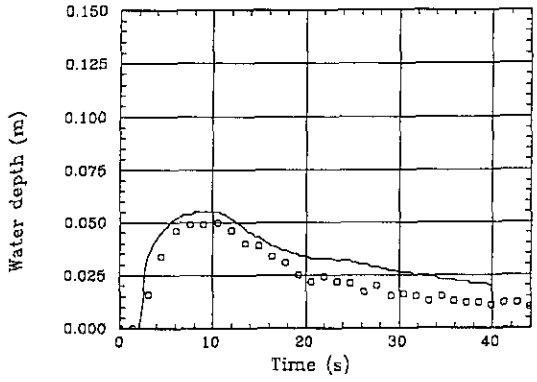

FIG. 22. Test case $S_{0x} = 0.01$, $h_1 = 0.3$ m, $h_2 = 0.0$ m. Continuous line: Predicted values. Circles: Measured values. Section 3. TVD scheme.

Smaller values of the time step were tried with no significant improvement in the outcome. On the other hand, resolution in a finer grid (twice the number of cells in each direction) rendered the results more accurate. However, the cost of the computation with the finer grid made doubtful the interest that the extra accuracy obtained. The Euler integration in time used is not the best choice, but many successful schemes use it. Other more accurate time-stepping schemes are available [16] and their use could improve the overall scheme, provided that a reasonable relation between accuracy and efficiency is met.

The results obtained from the finite volume TVD scheme for the same problem are shown as a means to establish the numerical merits of the new scheme by comparison. In general, the numerical results from both methods are similar, which indicates that the errors are not due to the numerical scheme but, perhaps, to a too simple modelization of a very complicated problem.

6. CONCLUSIONS

Two-dimensional wave decomposition and multidimensional upwinding seem a promising method of solution for the 2D shallow water equations. Two wave models have been adapted to render the technique suited to hydraulic problems with shocks. As with the 1D TVD schemes, our experience with using the multidimensional upwind approach for the shallow water equations has closely followed that of the researchers solving the Euler equations (with both the advection schemes and wave models) showing the same properties as for that system of equations.

Although the procedure is more complicated and costly than present day generalizations of 1D upwinding techniques it is based on a triangular discretization and, by taking advantage of the triangles, the disadvantages can be overcome, making the schemes very competitive. The future for them then looks much more promising. They can clearly be applied to arbitrary geometries, a great advantage for hydraulic engineers working on practical problems, and there is a wide variety of possibilities concerning grid movement and adaption.

Future work is envisaged to find better ways to deal with the source terms present in the shallow water equations when applied to realistic problems, as well as more efficient schemes to treat the time integration in unsteady cases.

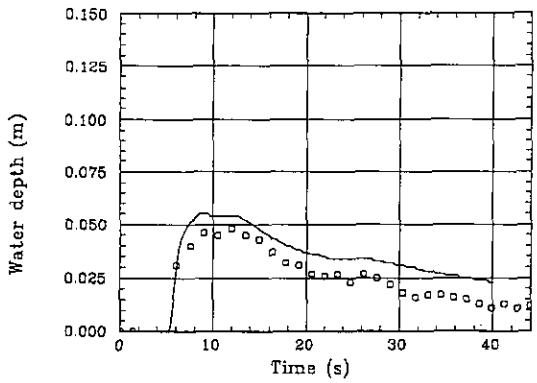

FIG. 23. Test case $S_{0x} = 0.01$, $h_1 = 0.3$ m, $h_2 = 0.0$ m. Continuous line: Predicted values. Circles: Measured values. Section 4. TVD scheme.

ACKNOWLEDGMENT

We thank Dr. Mike Baines for many useful and interesting discussions during the course of this work.

REFERENCES

1. F. Alcrudo and P. Garcia-Navarro, *Int. J. Numer. Methods Fluids* **16,** 489 (1993).
2. M. Baines, *Math. Comput.* to appear.
3. C. V. Bellos, J. V. Soulis, and J. G. Sakkas, *Adv. Water Resources* **14,** 31 (1991).
4. J. A. Cunge, F. M. Holly, and A. Verwey, *Practical Aspects of Computational River Hydraulics* (Pitman, London, 1980.)
5. H. Deconinck, R. Struijs, G. Bourgois, H. Paillere, and P. L. Roe, "Multidimensional Upwind Methods for Unstructured Grids," in *Unstructured Grid Methods for Advection Dominated Flows,* AGARD, Vol. 787 (1992).
6. Ch. Hirsch, *Natural Computation of Internal and External Flows. Vol. 2. Computational Methods for Inviscid and Viscous Flows* (Wiley, Chichester, 1990.)
7. R. J. Fennema, and M. H. Chaudhry, *J. Hydraul. Eng. ASCE* **116,** 1013 (1990).
8. P. Garcia-Navarro, and F. Alcrudo, *J. Hydraul. Eng. ASCE* **118,** 1359 (1992).
9. P. Garcia-Navarro and F. Alcrudo, in *Proceedings, XXV IAHR Congress Tokyo, 1993.*
10. M. E. Hubbard, *Numerical Analysis Report* **7/93,** Department of Mathematics, University of Reading, U.K., 1993.
11. P. L. Roe, *J. Comput. Phys.* **63,** 458 (1986).
12. P. L. Roe, "A Basis for Upwind Differencing of the Two-Dimensional Unsteady Euler Equations," in *Numerical Methods for Fluid Dynamics II,* edited by K. W. Morton and M. J. Baines (Oxford Univ. Press, London, 1986).

13. P. L. Roe, R. Struijs, and H. Deconinck, *J. Comput. Phys.*, to appear.
14. M. Rudgyard, *Multidimensional Wave Decompositions for the Euler Equations*, VKI Lecture Series, Computational Fluid Dynamics, 1993.
15. R. Struijs, P. L. Roe, and H. Deconinck, *Fluctuation Splitting Schemes for the 2D Euler Equations*, VKI Lecture Series 1991-01, Computational Fluid Dynamics, 1991.
16. C. B. Vreugdenhil and B. Koren (Eds.), *Numerical Methods for Advection-Diffusion Problems* Notes on Numerical Fluid Mechanics, Vol. 45, Braunschweig, Vieweg, 1993.